International Journal of Nanomedicine

Dovepress
open access to scientific and medical research

Open Access Full Text Article

ORIGINAL RESEARCH

Sequentially Released Liposomes Enhance Anti-Liver Cancer Efficacy of Tetrandrine and Celastrol-Loaded Coix Seed Oil

Yunyan Chen[1,2], Ziwei Zhang[1,2], Zhilei Qian[3], Rui Ma[1,2], Minna Luan[1,2], Yu Sun[1]

[1]School of Pharmacy, Wannan Medical College, Wuhu, 241002, People's Republic of China; [2]Institute of Synthesis and Application of Medical Materials, Wannan Medical College, Wuhu, 241002, People's Republic of China; [3]The Affiliated Brain Hospital of Nanjing Medical University, Nanjing, 210029, People's Republic of China

Correspondence: Yunyan Chen; Yu Sun, School of Pharmacy, Wannan Medical College, Wuhu, 241002, People's Republic of China, Tel +86 553 3932492, Email cyy1206@163.com; whsunyu@163.com

Background: A sequential release co-delivery system is an effective strategy to improve anti-cancer efficacy. Herein, multicomponent-based liposomes (TET-CTM/L) loaded with tetrandrine (TET) and celastrol (CEL)-loaded coix seed oil microemulsion (CTM) were fabricated, which showed synergistic anti-liver cancer activities. By virtue of Enhanced Permeability and Retention (EPR) effect, TET-CTM/L can achieve efficient accumulation at the tumor site. TET was released initially to repair abnormal vessels and decrease the fibroblasts, and CTM was released subsequently for eradication of tumor tissue.

Methods: TEM (transmission electron microscopy) and DLS (dynamic light scattering) were adopted to characterize the TET-CTM/L. Flow cytometry was adopted to examine the cellular uptake and cytotoxicity of HepG2 cells. The HepG2 xenograft nude mice were adopted to evaluate the anti-tumor efficacy and systemic safety of TET-CTM/L.

Results: TEM images of TET-CTM/L showed the structure of small particle size of CTM within large-size liposomes, indicating that CTM can be encapsulated in liposomes by film dispersion method. In in vitro studies, TET-CTM/L induced massive apoptosis toward HepG2 cells, indicating synergistic cytotoxicity against HepG2 cells. In in vivo studies, TET-CTM/L displayed diminished systemic toxicity compared to celastrol or TET used alone. TET-CTM/L showed the excellent potential for tumor-targeting ability in a biodistribution study.

Conclusion: Our study provides a new strategy for combining anti-cancer therapy that has good potential not only in the treatment of liver cancer but also can be applied to the treatment of other solid tumors.

Keywords: celastrol, tetrandrine, sequentially released liposomes, anti-liver cancer

Introduction

Liposome-based nano drug delivery systems are emerging as one of the most promising anticancer drugs, but still face increasing challenges in the dilemma of chemotherapy.[1,2] On account of the EPR effect, the nano-drug delivery system can reduce the targeting toxicity and enhance the accumulation at the tumor site compared with conventional chemotherapy.[3–6] Commercially available liposomes, such as Doxil®, Marqibo®, DepoCyt® were studied in alternative chemotherapy, have already shown significant advantages in reducing systemic cytotoxicity.

Tumor-associated fibroblasts (CAFs) can induce massive collagen deposition and scaffold protein remodeling, resulting in dense tissue and increased osmotic pressure.[7,8] This obstacle hinders the intra-tumoral permeation and therapeutic efficacy of nanomedicine. Therefore, reasonable intervention of CAFs may not only inhibit the tumor-promoting efficacy but also normalize the intra-tumoral delivery pathway of nanomedicine by regulating the tumor microenvironment to achieve better therapeutic efficacy.[9]

Tetrandrine, an alkaloid that was extracted from traditional Chinese medicine herb *Stephania tetrandra S*, displayed significant anti-hepatic fibrosis efficacy. It has been reported that tetrandrine can inhibit the production of TLR-related ligand,

Received: 3 November 2023
Accepted: 16 January 2024
Published: 23 January 2024

which in turn inhibits TLR4-mediated secretion of inflammatory factors such as TGF-β_1 and decreases TGF-β_1-mediated activation of fibroblasts. Tetrandrine can also inhibit the proliferation of hepatic fibroblasts indirectly by down-regulating the expression of TIMP-1 and MMP, and then reduce the deposition of collagen and the expression of fibrosis-related genes in the extracellular matrix.[10–13] In addition, TET has a very broad range of different pharmacological activities, including anti-inflammatory, anti-rheumatoid arthritis, anti-adipogenic, and so on.[14–25]

Celastrol is one of the main active components of *Tripterygium wilfordii*, which is one of five promising natural drug molecules and has shown excellent activities in the treatment of various cancers, inflammation, and so on. However, due to the non-selective distribution of the drug, its hepatotoxicity, nephrotoxicity, and immunosuppressive effects have severely limited the clinical application of celastrol. In our previous study, we have prepared a celastrol-loaded coix seed oil microemulsion, which has excellent anti-tumor efficacy.[26–32]

In this study, by constructing a TET and celastrol-loaded coix seed oil microemulsion lipid complex (TET-CTM/L) (Scheme 1). TET can be initially released to target CAFs precisely to restore the abnormal vessel and decrease the fibroblast at the tumor site. Meanwhile, CTM was released subsequently to improve the anti-tumor efficacy, which can achieve deep penetration by virtue of small size at the tumor site. This project integrates the advantages of "normalization window" and small-sized microemulsions which promotes the efficient penetration of anti-tumor components, it provides a new idea for further improving the delivery efficiency and anti-tumor efficacy of multi-component nano-drug delivery system of traditional Chinese medicine (TCM).

Materials and Methods

Materials

Celastrol and tetrandrine were provided by the Aladdin Technology Co., LTD. (purity >98%, China). Coix seed oil was procurement of goods from Yuanye Biotechnology Co., Ltd. (Shanghai, China). HS15 was purchased from BASF Co., Ltd. (Ludwigshafen, Germany). PEG 400, $CHCl_3$, Methanol, and DMSO were all obtained from Sinopharm Group Co., Ltd. (Shanghai, China). DPPC, S-lysoPC, and DSPE-mPEG$_{2k}$ were purchased from AVT Co., Ltd. (Shanghai, China). DMEM, fetal bovine serum (FBS), EDTA-0.25% trypsin solution, and phosphate buffer were obtained from Gibco Co., Ltd. (California, USA). BestBio® Reagent was provided by BestBio Co., Ltd. (Shanghai, China). LysoTracker Red was purchased from Abcam Co., Ltd. (Massachusetts, UK). Human liver cancer (HepG2) cells were bought from Heyuan Biotechnology Co., Ltd. (Shanghai, China). The water used is pure water. Unless otherwise noted, all other chemicals and reagents adopted in this study were of analytical grade.

Animals

Nude mice (BALB/c, 25 ± 2 g) were procurement of goods from Jiangsu Huachuang Cigna Pharmaceutical Technology Co., LTD. Before the trial, all the Nude mice were fed on light–dark cycle (12 h) and acclimated for at least a week with free access to water and food. Animal welfare and experimental procedures were strictly in accordance with the Guide for the Care and Use of Laboratory Animals (US National Research Council, 2011) and the related ethics regulations of Wannan Medical College, and this protocol was approved by the Animal Experiment Ethics Committee of Wannan Medical College (No. LLSC-2022-044).[33,34]

Preparation and Characterization of TET-CTM/L

CTM is prepared according to the following method: Firstly, HS 15 (450 mg), PEG 400 (150 mg), coix seed oil (400 mg), and celastrol (10 mg) were weighed precisely and then stirred for 4 h at 400 rpm under heating conditions at 42°C. After stirring well, pure water (10 mL) was added to obtain celastrol-loaded coix seed oil microemulsion (CTM).[33,34]

TET-CTM/L was prepared according to the following method: DPPC (18.00 mg), S-lysoPC (1.60 mg), DSPE-mPEG$_{2k}$ (4.00 mg), and TET (5.00 mg) were weighed precisely and add 10 mL of $CHCl_3$ to dissolve completely.[34] Using a rotary evaporator, after vacuum evaporation for 2.5 h at 37°C, the prepared CTM was hydrated at 50°C for 3 h at atmospheric pressure to produce TET and celastrol-loaded coix seed oil microemulsion lipid complex.

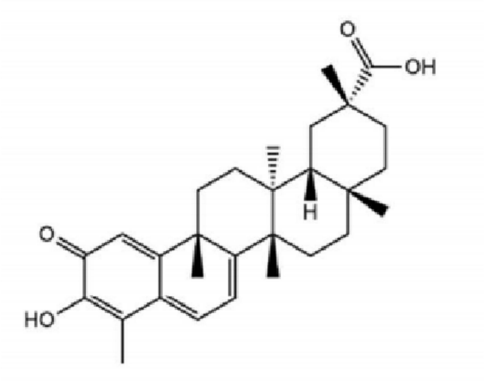

Celastrol

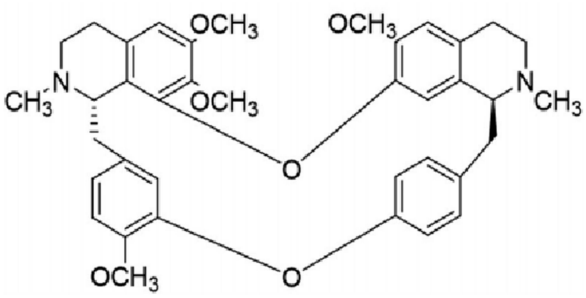

Tetrandrine

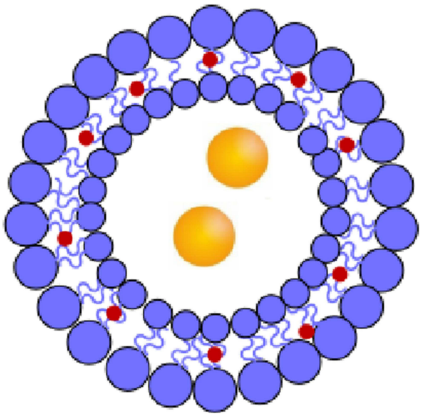

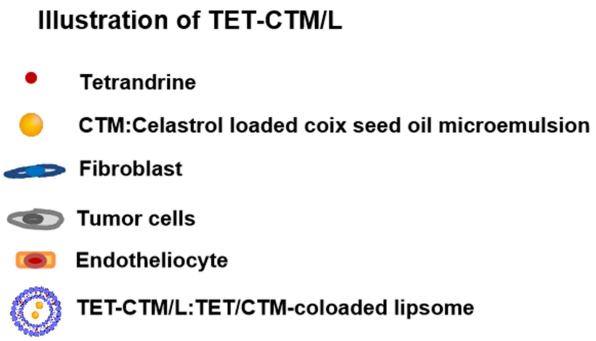

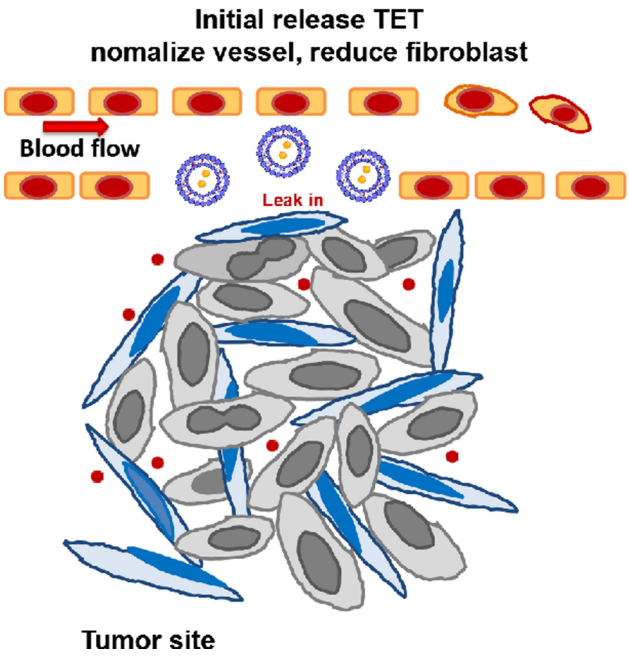

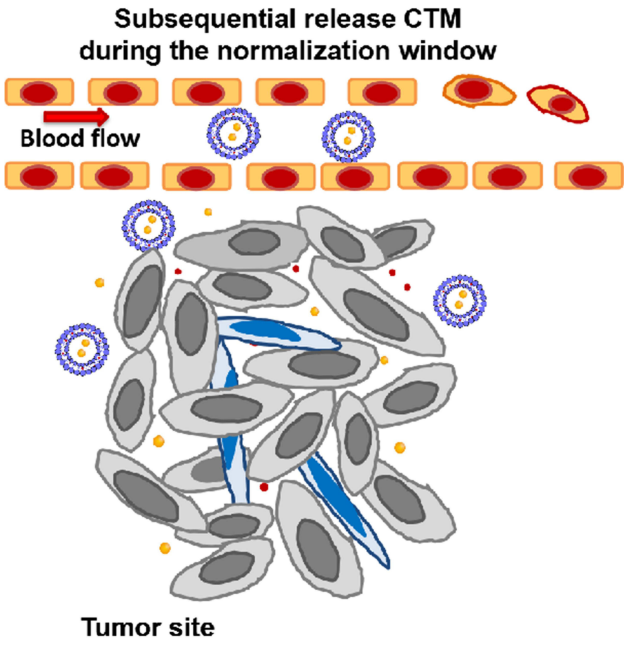

Scheme 1 TET-CTM/L with a "small-in-large" structure is composed of tetrandrine and celastrol-loaded coix seed oil microemulsion. Due to a dual-encapsulation of microemulsion and liposome, tetrandrine could be released from TET-CTM/L rapidly. However, celastrol and coix seed oil are capable of slower release. When TET-CTM/L accumulates at the tumor site, the initial released tetrandrine restores the abnormal vessel and decreases the fibroblast of the tumor site to open a "normalization window". The subsequent liposomes as well as released celastrol and coix seed oil.

TET/L is prepared based on the preparation of TET-CTM/L. Pure water replaced the prepared CTM, followed by hydrated at 50°C for 3 h at atmospheric pressure to produce TET/L.[34]

Dynamic light scattering (DLS) laser scattering particle size analyzer (Nano-Z, Malvern, UK) was adopted to measure the zeta potential and particle size of TET-CTM/L. Transmission electron microscope (TEM, JEM-2100F, JEOL, Japan) was adopted to observe the morphology of TET-CTM/L.[33–37]

Drug Measurement by HPLC

The chromatographic conditions for celastrol were as follows: Wonda Cract ODS-2 column (4.6 × 250 mm, 5 μm); mobile phase, Methanol–water–0.1% glacial acetic acid (90:10); detection wavelength, 426 nm.

The chromatographic conditions for tetrandrine were as follows: Wonda Cract ODS-2 column (4.6 × 250 mm, 5 μm); mobile phase, Methanol–water–0.03 triethylamine (85:15); detection wavelength, 215 nm.

The calculations of encapsulation efficiency (EE) and loading efficiency (LE) of celastrol and tetrandrine were as follows:[33–37]

$$\mathrm{EE}\ (\%) = \mathrm{W}_{\text{encapsulated CEL/TET}} / \mathrm{W}_{\text{feeding CEL/TET}} \times 100\%$$

$$\mathrm{LE}\ (\%) = \mathrm{W}_{\text{encapsulated CEL/TET}} / \mathrm{W}_{\text{weight of the freeze-dried TET-CTM/L}} \times 100\%$$

Drug Release in vitro

Determination of celastrol and tetrandrine release in TET-CTM/L using a classical dialysis method.[33–37] 1 mL of TET-CTM/L was precisely pipetted into a dialysis bag, then incubated in a solution containing a mixture of PBS and Tween 80 (0.5%) at rate of 60 r/min. At predetermined time intervals (0–48 h), aspirate 50 μL of PBS solution and add an equal amount of fresh medium supplement. Determination of cumulative release of celastrol and tetrandrine from TET-CTM/L by HPLC.

Cell Culture

A cell incubator with 5% CO_2 and 95% humidity at 37°C was adopted to culture human liver cancer cells (HepG2), which were cultured with DMEM containing 10% FBS (v/v), streptomycin and penicillin (1%, 100 μg/mL).

Intracellular Delivery and Cellular uptake

HepG2 (5×10^5) cells were seeded into 6-well cell culture plates and incubated for 24 h. All the treatments were labeled with fluorescein isothiocyanate (FITC). To detect the cellular uptake of FITC/CT-MEs/Lip, FITC, FITC/C-MEs, and FITC/C-MEs/Lip were adopted as controls. FITC, FITC/C-MEs, FITC/C-MEs/Lip, and FITC/CT-MEs/Lip were administered to HepG2 cells at 1 mL/well (10 μM, calculated as FITC concentration) and then incubated for 2 h.[33–37] The fluorescence intensity of all treatments was observed by flow cytometry (BD FACSVerse, New Jersey, USA).

HepG2 (2×10^5) cells were diluted and seeded into laser confocal glass dishes. DiD, DiD-MEs, and DiD-C-MEs/L were administered at 1 mL/well (5 μM, calculated as DiD concentration) and then incubated for 2 h. LysoTracker Red was added and followed by incubation for 30 min and finally observed by confocal laser scanning microscopy (Leica, TCS SP8, Germany).

Cytotoxicity

HepG2 cells in logarithmic growth phase were collected to seed in 96-well plates and incubated for 24 h. All celastrol treatments were divided into CEL, TET, CTM, TET/L, and TET-CTM/L at a concentration of 0.675~20 μg/mL as calculated by celastrol. After 24 h, MTT (5 mg/mL) was added and followed by incubation for 4 h at 37°C. DMSO was added (100 μL/well), and the absorbance (A) value of was detected by a microplate reader at 490 nm (Tecan M200Pro, Thermo, USA).[33,34]

Cell Apoptosis Induction

The BestBio® Reagent Apoptosis Kit (BestBio, China) was adopted to detect the apoptosis in HepG2 cells by TET-CTM/L. HepG2 cells (2×10^5) were seeded in 6-well plates and incubated at 37°C for 24 h. The concentration of celastrol in all treatments was set at 2 μg/mL, and the incubation time was 12 h. The apoptosis of HepG2 cells was measured by flow cytometry.

Xenograft Tumor Models

The HepG2 cell suspension containing 2×10^7 cells was injected subcutaneously into the right hind limb of mice to establish a HepG2 xenograft tumor model. The tumor size was measured with a Vernier caliper, calculated as $V = (L \times W^2)/2$, where L is the vertical length and W is the vertical width.

In vivo Imaging

The HepG2 xenograft nude mice were adopted and randomly divided into 4 groups in case the tumor volume increased to 120 mm^3. The experimental groups were as follows: DiD, DiD+TET, DiD/C-MEs, TET-DiD/L, and DiD-C-MEs/L. 0.2 mL of each treatment was intraperitoneally injected into the HepG2 xenograft nude mice, and the dose of DiD was 30 μg/mL.[33,34] After isoflurane anesthesia, NIR images were obtained using an in vivo imaging system (PerkinElmer, IVIS Lumina LT, USA). Region-of-interest (ROI) function was used to measure the fluorescence after administration at the stated delivery time. After treatment for 12 hours, the mice were euthanized to collect the fluorescent images of major normal organs including heart, liver, spleen, lung, kidney, and tumor tissues, adopting the in vivo imaging system.[33–38]

Antitumor Efficacy and Systemic Safety

Thirty-five HepG2 xenograft-bearing nude mice with a mean tumor size of approximately 100 mm^3 were injected subcutaneously once every two days with CEL, CEL+TET, CTM, TET/L, and TET-CTM/L at concentration of 1.5 mg/kg as calculated by celastrol.[33–38] Tumor size and body weight of each group of mice were recorded daily. Each nude mouse was subjected to eye blood sampling and collection of heart, liver, spleen, lung, kidney, and the tumor tissues. All blood (or serum) collected will be used for analysis of liver/kidney function and blood route analysis. Paraffin embedding and pathological sectioning were performed on the peeled tumor tissue and then stained with hematoxylin and eosin (H&E). Finally, a fluorescence microscope was used to observe the images of the stained sections.

Tumor Microenvironment Characterization

Based on our previous study, α-SMA can be used to characterize the tumor microenvironment. Tumor sections of all celastrol treatments were deparaffinized via dimethylbenzene thrice, followed by water-alcohol solutions rinsing, and then incubated with 0.1% Triton X-100 (15 min) and finally blocking with 1% BSA (30 min).[34] All tumor sections were incubated with primary polyclonal human α-SMA antibody (Abcam, UK) and then further incubated with Alexa Fluor 555-conjugated secondary antibody both for 1 h. Staining with DAPI (30 min), fixing with 4% paraformaldehyde (15 min), and subsequent observation by CLSM were conducted.[34,38]

Data Analysis

All data were analyzed using GraphPad Prism Software 9 and expressed as mean ± standard deviation (SD). $*P < 0.05$ indicates statistical difference, $**P < 0.01$ indicates extreme statistical significance.

Results and Discussion

Characterization of TET-CTM/L

TET-CTM/L is comprised of two constitutes: tetrandrine encapsulated in the lipid layer and celastrol-loaded coix seed oil microemulsion loaded within liposome (Scheme 1). The particle size of CTM and TET-CTM/L were approximately 25 nm and 120 nm, respectively (Figure 1A). The zeta potentials of CTM and TET-CTM/L were −0.374 ± 0.073 mV and −0.204 ± 0.067 mV. In particular, the appearance of CTM is spherical, and TEM images of TET-CTM/L showed the structure of small

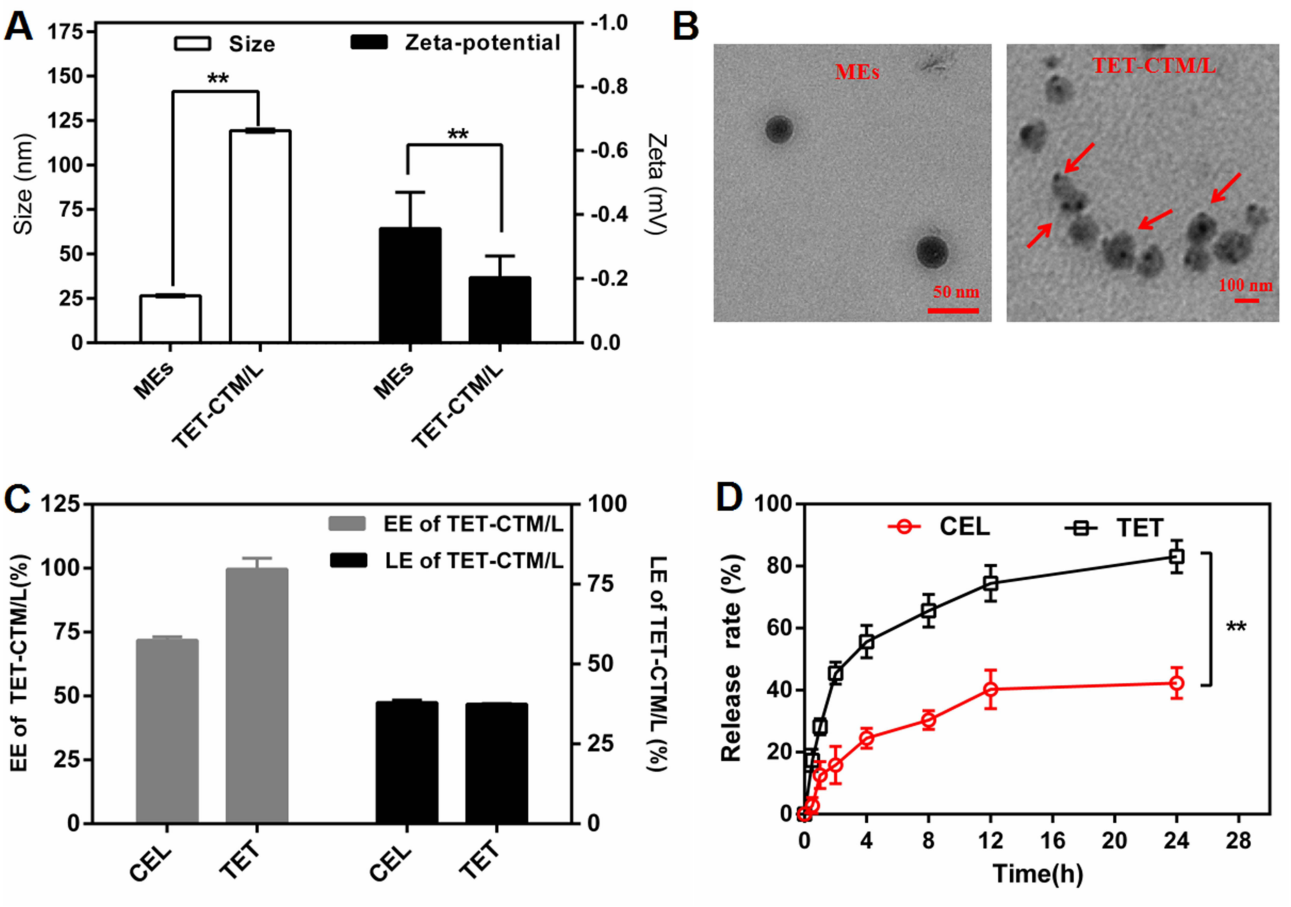

Figure 1 Characterization of TET-CTM/L (**A**) Size and Zeta-potential of TET-CTM/L by DLS. Data are represented as mean ± SD; n=3. $^{**}P<0.01$. (**B**) TEM images of TET-CTM/L. The red arrows represent the liposome-internal CTM. (**C**) Drug encapsulation efficiency and loading efficiency of TET-CTM/L. Data are represented as mean ± SD; n=3. (**D**) In vitro accumulative drug release of TET-CTM/L within 24 h (pH 7.4). Data are represented as mean ± SD; n = 3. $^{**}P < 0.01$.

particle size of CTM within large particle size of liposomes, indicating that CTM can be encapsulated into liposomes by film dispersion method (Figure 1B).[33,34] Therefore, TET-CTM/L liposome complexes can have two optimal particle sizes simultaneously. The encapsulation efficiency (EE) of celastrol and TET in TET-CTM/L were 71.86% and 98.45%, separately. Compared with TET, the EE of celastrol decreased gradually, which may be related to the increase in excipients and the structure of lipid bilayer. The drug loading efficiency (LE) of celastrol and tetrandrine in TET-CTM/L was 37.921% and 37.425% (Figure 1C). According to the combined therapy of tetrandrine and celastrol in vivo, we preliminarily realized the necessity of sustained release administration to achieve better anti-cancer efficacy. In this study, the staged-release of celastrol and tetrandrine in TET-CTM/L was verified by classical dialysis method in vitro.[34] After incubation for 24 h, 83.10% of tetrandrine was released from TET-CTM/L in PBS at pH 7.4, which was 1.96 times faster than celastrol, the slower release rate of celastrol indicates that TET-CTM/L can be used as a model for stepwise drug release (Figure 1D). It offers the possibility that TET-CTM/L could release tetrandrine firstly to restore abnormal blood vessels and thus to reduce fibroblasts, and meanwhile to open a "normalization window" for subsequent retention of CTM in tumor tissue.[38]

Internalization and Intracellular Delivery of TET-CTM/L

We evaluated the cellular uptake of various celastrol treatments in the internalization and intracellular delivery study. The intracellular fluorescence of FITC/C-MEs and FITC/CT-MEs/Lip was more intense than that of free FITC, suggesting enhanced endocytosis of HepG2 cells by nanoparticles ($^{**}p < 0.01$) (Figure 2A and B).[33–38] In particular, the uptake fluorescence intensity of FITC/CT-MEs/Lip to HepG2 cells was (344.00 ± 6.56), it was 1.11-fold higher

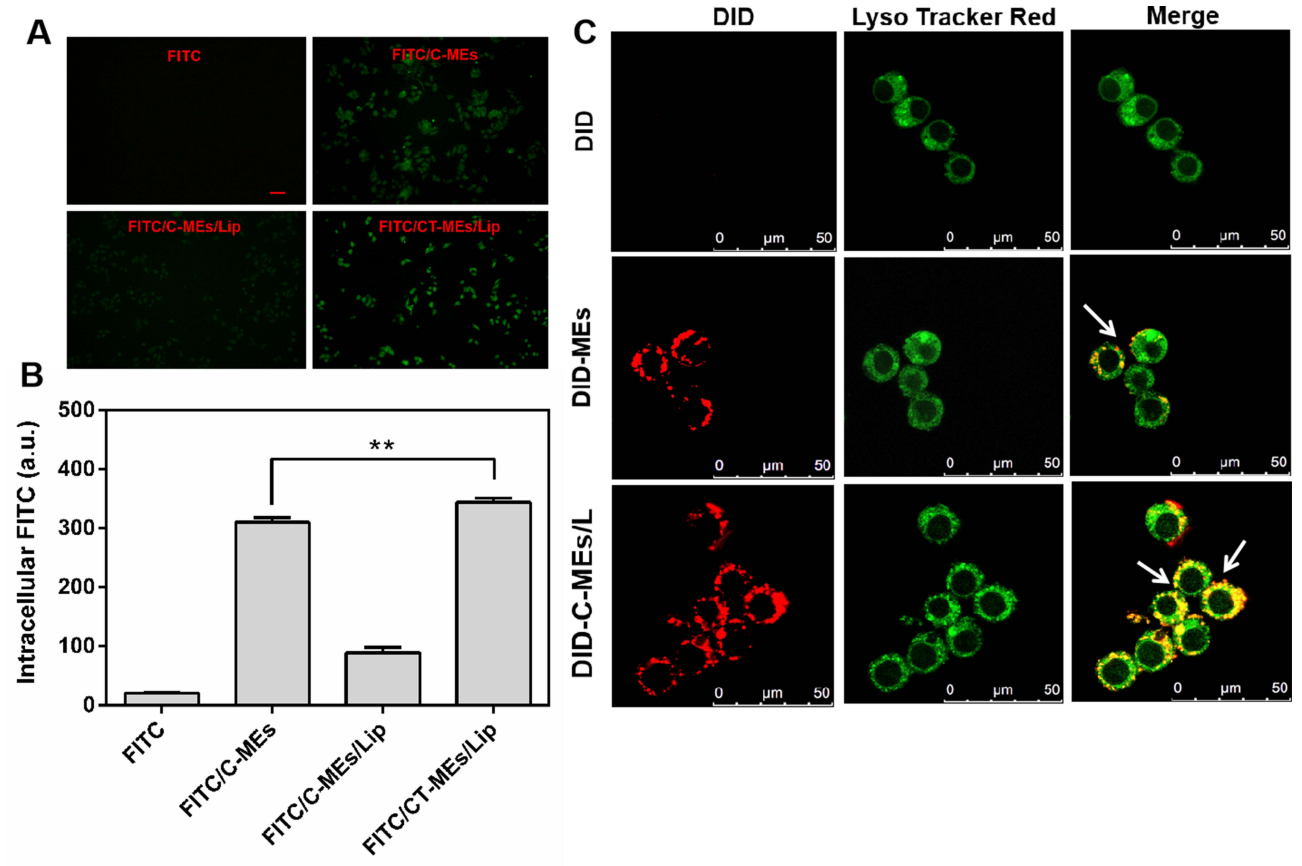

Figure 2 Cellular uptake. (**A**) Fluorescent images of HepG2 cells incubated with FITC, FITC/C-MEs, FITC/C-MEs/Lip, and FITC/CT-MEs/Lip for 3 h (Scale bar: 100 μm). (**B**) Mean fluorescence intensity of HepG2 cells were analyzed by flow cytometry after incubation with preparations for 3 h (n = 3, $^{**}p < 0.01$). Data are represented as mean ± SD. (**C**) Intracellular delivery of DiD, DiD-MEs, and DiD-C-MEs/L within HepG2 cells observed using CLSM (custom pseudo-color). The arrows represent treatments entrapped in the endo/lysosomes (Scale bar: 50 μm).

than that of FITC/C-MEs (310.33 ± 8.33), indicating that small-sized nanoparticles have inherent advantages in internalization.

Laser confocal microscopy was adopted to examine the intracellular localization of various celastrol treatments. DiD was adopted to label various celastrol treatments with red fluorescence, and LysoTracker Red was adopted to label the endo/lysosomes with green fluorescence (custom pseudo-color). Notably, HepG2 cells treated with FITC/CT-MEs/Lip indicated distinct yellow fluorescence, suggesting that TET-CTM/L may be retained by endo/lysosomes (Figure 2C).[39]

Cell Apoptosis Induction

To confirm our new strategy for combining anti-cancer therapy, Annexin V-PE/7-AAD staining method was adopted to detect the apoptosis in HepG2 cells caused by CEL, CEL + TET, CTM, TET/L, and TET-CTM/L.[40] HepG2 cells were treated with celastrol at a dose of 2 μg/mL, and after 12-h incubation, the apoptosis of HepG2 cells was detected.[33,34] The apoptosis rates of HepG2 cells in CEL, CEL+TET, CTM, TET/L, and TET-CTM/L were (64.6 ± 2.79)%, (65.6 ± 4.57)%, (63.3 ± 1.04)%, (41.4 ± 3.52)%, and (71.2 ± 1.07)%, respectively (Figure 3A and B). Notably, the HepG2 cells all exhibited excellent total apoptosis rates, mainly due to the synergistic anti-tumor efficacy of nano drug delivery system and inherent advantages in internalization. In particular, our study verified that TET-CTM/L can significantly induce massive apoptosis in HepG2 cells, suggesting that TET-CTM/L is expected to achieve excellent anti-tumor efficacy in vivo.

Antiproliferative Effects in vitro

Here, to validate the synergistic anti-tumor efficacy of TET-CTM/L, all celastrol treatments including CEL, CEL+TET, CTM, and TET/L were taken as controls, our study evaluated the cytotoxicity of TET-CTM/L against HepG2 cells.[41,42]

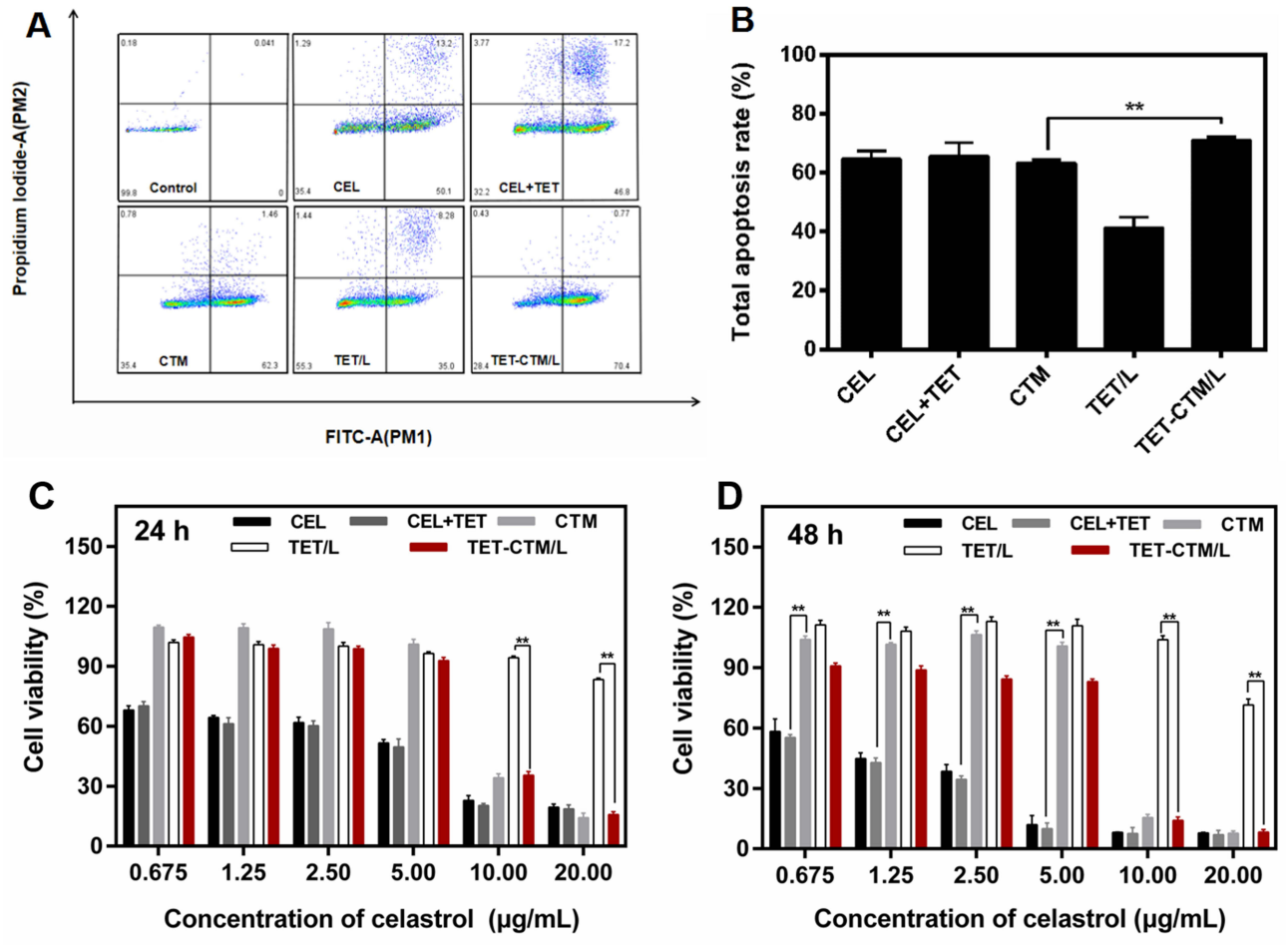

Figure 3 Cell apoptosis and cytotoxicity (**A**) Apoptosis ratio of HepG2 cells treated with various celastrol treatments at concentration of 2 μg/mL for 12 h. (**B**) The quantitative analysis of total apoptosis rate of HepG2 cells treated with various celastrol treatments. Data are represented as mean ± SD; n = 3. $^{**}P < 0.01$. Cytotoxicity of various celastrol treatments against HepG2 cells for (**C**) 24 h and (**D**) 48 h. Data are represented as mean ± SD; n = 6. $^{**}P < 0.01$.

All various celastrol treatments had obvious proliferation inhibition of HepG2 cells, meanwhile we found that the intensity of proliferation inhibition increased significantly with the increase in celastrol concentration after treatment for 24 and 48 h (Figure 3C and D). The IC_{50} values of various celastrol treatments against HepG2 cells for 24 h were 3.31 ± 0.64, 2.99 ± 0.48, 9.04 ± 0.88, 34.47 ± 1.63, 8.89 ± 0.55 μg/mL, respectively. The IC_{50} values of various celastrol treatments against HepG2 cells for 48 h were 1.04 ± 0.14, 0.92 ± 0.12, 9.14 ± 1.88, 21.03 ± 1.83, 6.90 ± 0.60 μg/mL, respectively. It is worth noting that the antiproliferative effect of TET-CTM/L against HepG2 cells in vitro indicates that TET-CTM/L has a significant sustained release of celastrol on the basis of good anti-tumor efficacy.

Biodistribution

To demonstrate the biodistribution of TET-CTM/L in the NIR in vivo imaging system,[43,44] all various celastrol treatments were labeled as DiD+TET, DiD/C-MEs, TET-DiD/L, and DiD-C-MEs/L, DiD were adopted to act as controls.[33–38] DiD group exhibited almost no accumulation at the tumor site between 1~8 h, and the fluorescence intensity was weaker in contrast to other Did treatments. DiD + TET group exhibited weak fluorescence at 6 h and meanwhile the accumulation increased gradually at the tumor site. At 1 h, DiD-C-MEs/L exhibited aggregation at the tumor site. After 4 h, DiD-C-MEs/L group was observed the highest fluorescence intensity at the tumor site, demonstrating that DiD-C-MEs/L can achieve efficient accumulation at the tumor site by virtue of EPR effect in vivo (Figure 4A). The NIR images of isolated organs showed basically no accumulation in the heart, lung, and kidney of all various DiD treatments, while both DiD-C-MEs and DiD-C-MEs/L groups accumulated in the spleens (Figure 4B). The NIR images

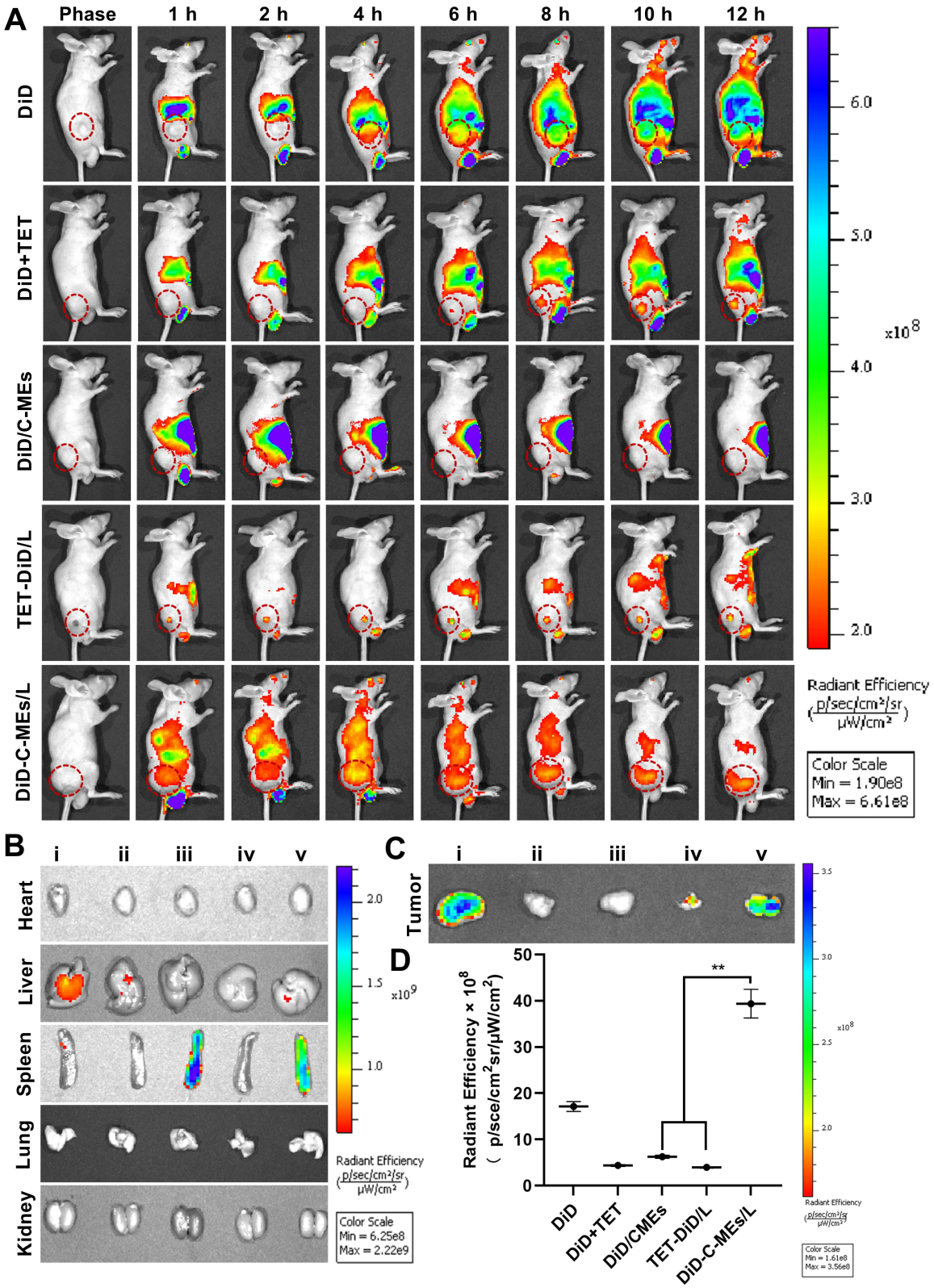

Figure 4 Investigation of biodistribution (**A**) Distribution of NIR signal on nude mice treated with various DiD-labeled formulations at the predetermined intervals. (**B**) Fluorescence images of normal organs at 12 h post-injection. (**C**) Fluorescence images of tumor tissues at 12 h post-injection. (**D**) Quantitative analysis of fluorescence in the tumor tissues after 12 h of the administration. Data are represented as mean ± SD, n=3. $^{**}p < 0.01$. (i), (ii), (iii), (iv) and (v) represent DiD, DiD+TET, DiD/C-MEs, TET-DiD/L and DiD-C-MEs/L, respectively.

of tumors showed that each group exhibits a certain degree of tumor accumulation. Related to the EPR effect, DiD-C-MEs/L group showed the strongest fluorescence intensity among all various Did treatments (Figure 4C). In our study, we also evaluated the fluorescence intensity quantitatively of isolated tumors after the administration of various Did treatments (Figure 4D). In particular, DiD-C-MEs/L group had the highest fluorescence intensity and showed significant differences compared to the DiD-C-MEs and TET-DiD/L groups. Additionally, DiD-C-MEs/L group showed the excellent potential for tumor-targeting ability.

Evaluation of Antitumor Efficacy

Adopting saline, CEL, CEL+TET, CTM, and TET/L as controls, the antitumor efficacy of TET-CTM/L in vivo was studied. The nude mice were intraperitoneally injected once every 2 days, at a dosage of 1.5 mg/kg for all various celastrol treatments.[33,34]

Changes in tumor size of nude mice treated with all various celastrol treatments showed that the TET-CTM/L group can significantly inhibit tumor growth (Figure 5A). The TET-CTM/L group has the most prominent tumor inhibition rate after being treated with various treatments at day 24 post-xenograft implantation, with a tumor inhibition rate of 86.37% (Figure 5B). We also plotted the weight of the nude mice during the whole period of treatment to assess systemic toxicity. The weight of the nude mice after being treated with various celastrol treatments showed a slightly decreasing trend compared to the saline group (Figure 5C). After a period of administration, the body weight remained stable and there were no significant differences between various celastrol treatments. The efficient accumulation of TET-CTM/L at the tumor site and the release of CTM with small particle size is the cornerstone of predominant anti-tumor efficacy. The nude mice treated with various celastrol treatments at the end of the observed period, the tumor weight of TET-CTM/L was the lowest among various celastrol treatments (Figures 5D and S1). Compared to the saline group, the H&E staining of tumor tissue of various celastrol treatments all showed a certain killing effect on HepG2 cells at the tumor site (Figure 5E). Notably, TET-CTM/L induced tumor nucleus division in the maximum necrotic area, showing overwhelming anti-tumor potency.

Evaluation of Systemic Safety

Drug toxicity seriously limits the application of antitumor drugs in clinical. Celastrol also faces the following barriers: high toxicity, poor solubility, and narrow therapeutic window.[33,34] All the reasons above severely limit the clinical application of celastrol. In this part of the study, all the blood and organ samples were detected to assess the potential toxicity of various kinds of celastrol treatments. There were no significant changes in liver and spleen index after treatment with TET-CTM/L, using HepG2 xenograft tumor-bearing mice (Figure 6A and B). For all the HE staining of major normal organs, TET-CTM/L hardly caused pathological changes in the heart, liver, spleen, lung, and kidney (Figure 6C). TET-CTM/L had negligible effects on white blood cells (WBC) and platelets (PLT) compared to normal nude mice, but after 14 days of treatment, TET-CTM/L had slightly altered the levels of hemoglobin (HGB) and red blood cells (RBC) (Figure 6D–G).

Normalization of Tumor Microenvironment

The underlying mechanism of the antitumor efficacy may be related to the normalization of tumor microenvironment by TET-CTM/L. TET-CTM/L with a "small-in-large" structure is composed of tetrandrine and celastrol-loaded coix seed oil microemulsion. Firstly, TET-CTM/L accumulates at the tumor site, and the initial release of tetrandrine restores abnormal blood vessels and reduces fibroblasts at the tumor site, opening a "normalization window". Subsequently, celastrol and coix seed oil (CTM) were released by the liposomes to kill tumor cells.

Cytokines are closely associated with the occurrence and development of tumor. CCL_2 is positively correlated with the degree of tumor malignancy. Recently, lots of studies have reported that CCL_2 is highly expressed in various tumor tissues and involved in the progress of tumor development and metastasis.[45,46] TNF-α, a pro-inflammatory cytokine formed by macrophages and monocytes, which can participate in normal inflammatory and immune responses.[47–53] In our study, TET-CTM/L can significantly inhibit the expression of chemokine CCL_2 and TNF-α, which is significantly

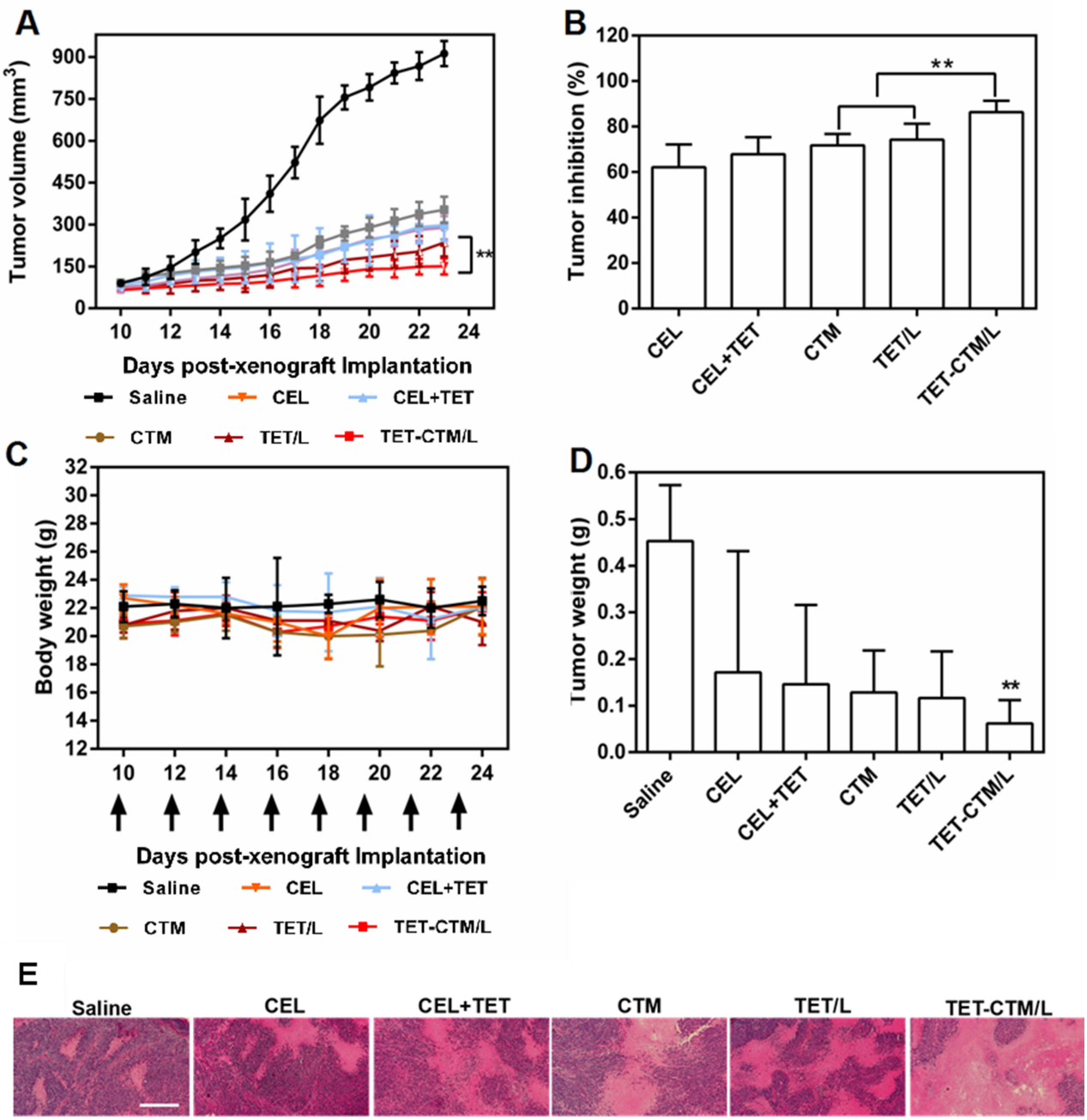

Figure 5 Antitumor efficacy in vivo (**A**) Changes in tumor volume of nude mice treated with different treatments. $^{**}p < 0.01$. (**B**) Tumor inhibition rate of nude mice treated with different treatments at day 24 post-xenograft implantation. $^{**}p < 0.01$. (**C**) Alterations in body weight of nude mice during the treatment. (**D**) Tumor weight of nude mice treated with various treatments at the end of the observed period. $^{**}p < 0.01$ vs celastrol. Data are represented as mean ± SD. (**E**) HE-stained images of the tumor slides of nude mice after treatment. The bar is 100 μm.

different from the saline group, indicating that TET-CTM/L may inhibit tumor growth by inhibiting the expression of CCL_2 and TNF-α (Figure 7A and B).

IFN-γ, which can activate M1-type tumor-associated macrophage TAMs, and meanwhile reduce CAFs by inhibiting the proliferation of tumor cells by blocking the pathway of angiogenesis.[54] IL-2, which also plays an important role in the immune response.[55,56] In particular, the expression of IFN-γ and IL-2 after treatment with TET-CTM/L was higher than the saline group, suggesting that the TET-CTM/L has an significant advantage in reducing the formation of CAFs (Figure 7C and D).

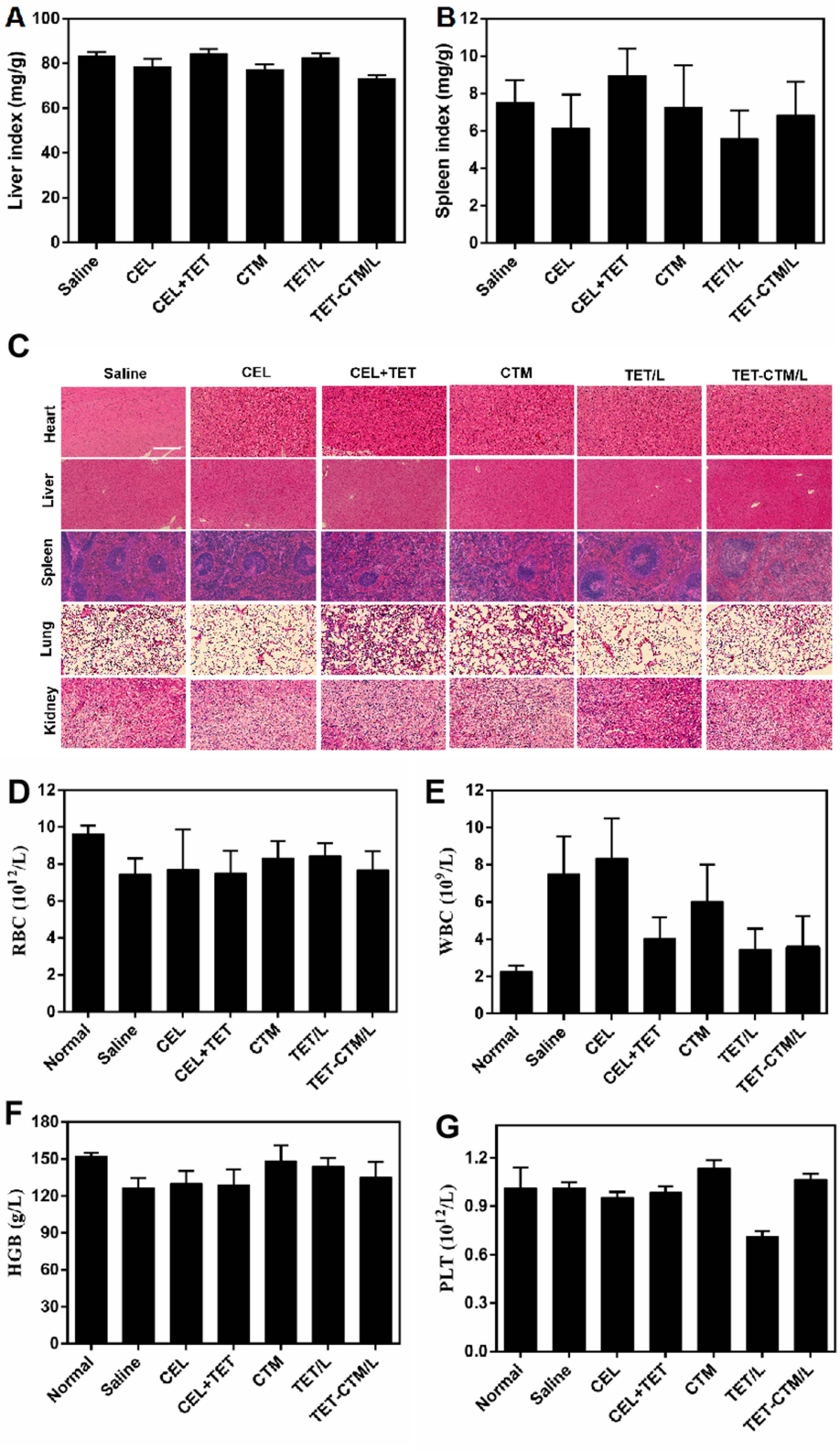

Figure 6 Evaluation on safety in vivo (**A**) Liver index and (**B**) spleen index of nude mice treated with various treatments. (**C**) Pathological section of HE-stained normal organs after treatment. The bar is 100 μm. (**D**) RBC (**E**) WBC (**F**) HGB and (**G**) PLT in blood samples of nude mice after 24 h of the last administration. Data are represented as mean ± SD; n = 5.

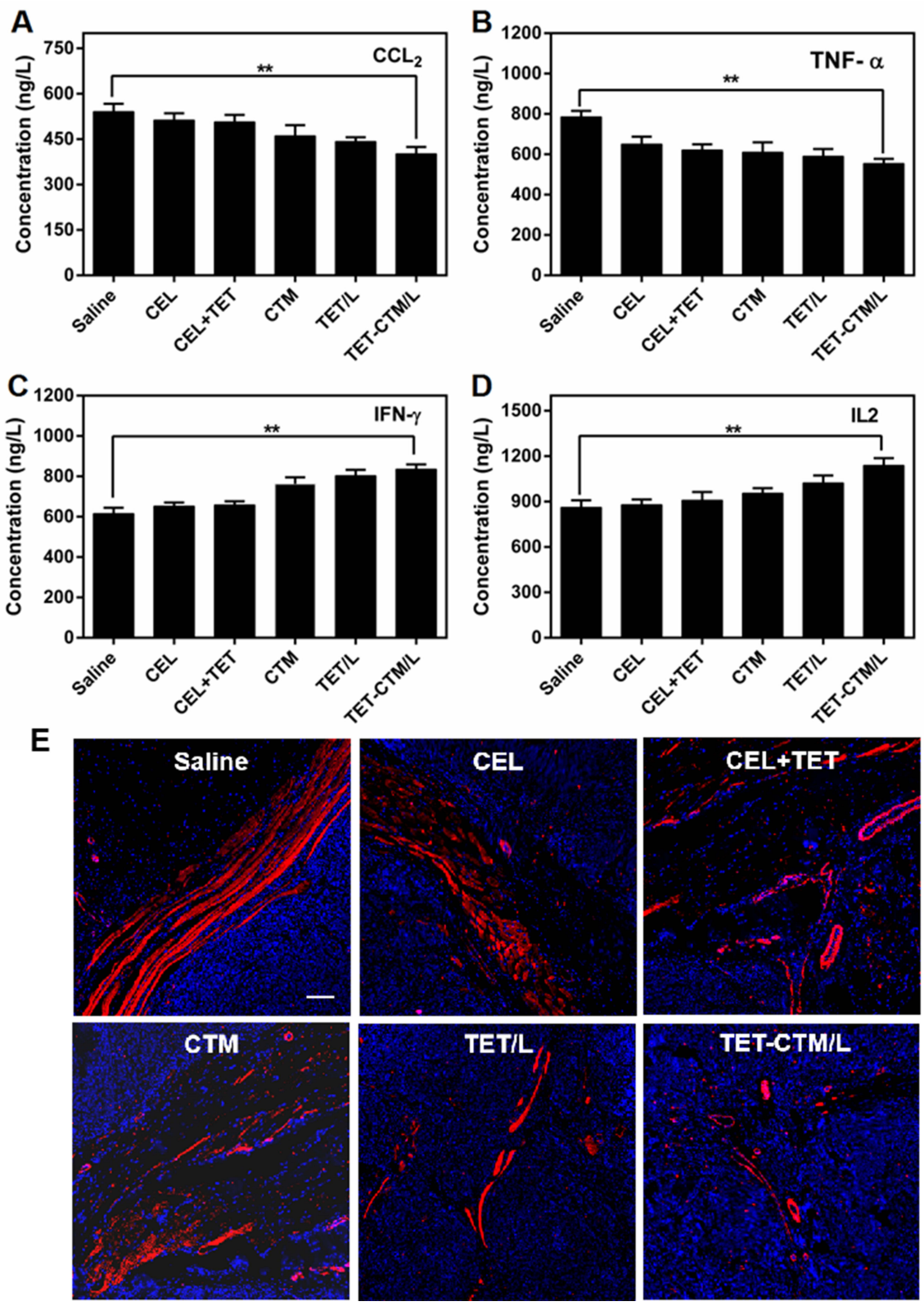

Figure 7 Normalization of tumor microenvironment. (**A**) CCL_2 (**B**) TNF-α (**C**) IFN-γ (**D**) IL-2 in serum of various celastrol treatments (n = 5, ± s) (**p <0.01) (**E**) α-SMA Assay. Fluorescence images of tumor section stained with anti-α-SMA primary antibody. The red represents the CAFs and the blue represents nucleus. The bar is 50 μm.

https://doi.org/10.2147/IJN.S446895 DovePress

CAFs, the major obstacle to tumor drug delivery, and fibroblasts were stained using α-SMA.[57] Notably, compared to the saline group, the level of α-SMA was significantly reduced after treatment with TET-CTM/L (Figure 7E). TET-CTM/L played a role in suppressing tumor angiogenesis by the initial release of tetrandrine to restore abnormal blood vessels and reduce fibroblasts at the tumor site, opening a "normalization window".[58]

Conclusions

In summary, we have developed a sequential release co-delivery system which is an effective strategy to improve anti-cancer efficacy. Herein, multicomponent-based liposomes (TET-CTM/L) loaded with tetrandrine (TET) and celastrol-loaded coix seed oil microemulsion (CTM) were fabricated, which showed synergistic anti-liver cancer activities by release of TET initially for regulation of the tumor microenvironment and CTM subsequently for eradication of tumor tissue. Our study provides a novel strategy for combined anti-cancer therapy that has promising potential not only in the treatment of liver cancer but also can be applied in the treatment of other solid tumors.

Acknowledgment

The study was supported by the Natural Science Foundation of China (22304132), Anhui Provincial Natural Science Foundation (2108085QH370), Anhui Provincial University Science Research Projects (2023AH040249, 2023AH051772) and Research Projects of University student entrepreneurship (S202210368069, S202310368083).

Disclosure

The authors report no conflicts of interest in this work.

References

1. Hassan S, Kamel A, Hashem H, et al. Drug delivery systems between metal, liposome, and polymer-based nanomedicine: a review. *Eur Chem Bull*. 2020;9(3). doi:10.17628/ecb.2020.9.91-102
2. Bharadwaj A, Gupta M, Shakya A. A critical review on nanotechnology: a technique in cancer detection and prophylaxis. *Nano Life*. 2023;13(03). doi:10.1142/S1793984423300042
3. Mpekris F, Papageorgis P, Polydorou C, et al. Sonic-hedgehog pathway inhibition normalizes desmoplastic tumor microenvironment to improve chemo-and nanotherapy. *J Control Release*. 2017;261:105–112. doi:10.1016/j.jconrel.2017.06.022
4. Bree C, Krooshoop J, Rietbroek R, et al. Hyperthermia enhances tumor uptake and antitumor efficacy of thermostable liposomal daunorubicin in a rat solid tumor. *Cancer Res*. 1996;56(3):563. doi:10.1097/00002820-199602000-00010
5. Glantz M, Lafollette S, Jaeckle K, et al. Randomized trial of a slow-release versus a standard formulation of cytarabine for the intrathecal treatment of lymphomatous meningitis. *J Clin Oncol*. 1999;17(10):3110–3116. doi:10.1161/01.CIR.62.3.485
6. Silverman J, Deitcher S. Marqibo (vincristine sulfate liposome injection) improves the pharmacokinetics and pharmacodynamics of vincristine. *Cancer Chemother Pharmacol*. 2013;71(3):555–564. doi:10.1007/s00280-012-2042-4
7. Fei X. Cancer associated fibroblasts (CAFs) in tumor microenvironment. *Front Biosci*. 2010;15(1):166–179. doi:10.2741/3613
8. Francesco E, Lappano R, Santolla MF, et al. HIF-1α/GPER signaling mediates the expression of VEGF induced by hypoxia in breast cancer associated fibroblasts (CAFs). *Breast Cancer Res*. 2013;15(4):R64. doi:10.1186/bcr3458
9. Jing J, Parekh H, Wei M, et al. Advances in analytical technologies to evaluate the quality of traditional Chinese medicines. *Trends Anal Chem*. 2013;44:39–45. doi:10.1016/j.trac.2012.11.006
10. Wong C, Seow W, O'Callaghan J, et al. Comparative effects of tetrandrine and berbamine on subcutaneous air pouch inflammation induced by interleukin-1, tumor necrosis factor and platelet activating factor. *Agents Actions*. 1992;36(1–2):112–118. doi:10.1007/BF01991238
11. Liu C, Gong K, Mao X, Li W. Tetrandrine induces apoptosis by activating reactive oxygen species and repressing Akt activity in human hepatocellular carcinoma. *Int J Cancer*. 2011;129(6):1519–1531. doi:10.1002/ijc.25817
12. Gao L, Feng Q, Zhang X, et al. Tetrandrine suppresses articular inflammatory response by inhibiting pro-inflammatory factors via NF-κB inactivation. *J Orthop Res*. 2016;34(9):1557–1568. doi:10.1002/jor.23155
13. Wang X, Yang Y, Yang D, et al. Tetrandrine prevents monocrotaline-induced pulmonary arterial hypertension in rats through regulation of the protein expression of inducible nitric oxide synthase and cyclic guanosine monophosphate-dependent protein kinase type 1. *J Vascular Surg*. 2016;64(5):1468–1477. doi:10.1016/j.jvs.2015.09.016
14. Liu B, Wang T, Qian X, et al. Anticancer effect of tetrandrine on primary cancer cells isolated from ascites and pleural fluids. *Cancer Lett*. 2008;268:166–175. doi:10.1016/j.canlet.2008.03.059
15. Bellik Y, Boukraâ L, Alzahrani H, et al. Molecular mechanism underlying anti-inflammatory and anti-allergic activities of phytochemicals: an update. *Molecules*. 2013;18:322–353. doi:10.3390/molecules18010322
16. Zhao H, Lou F, Li H, et al. Antinociceptive effect of tetrandrine on LPS-induced hyperalgesia via the inhibition of IKKb phosphorylation and the COX- 2/PGE2 pathway in mice. *PLoS One*. 2014;9:e94586. doi:10.1371/journal.pone.0094586
17. Lin Y, Chang C, Wu C, et al. Anti-nociceptive, anti-inflammatory and toxicological evaluation of Fang-Ji-Huang-Qi-Tang in rodents. *BMC Complement Altern Med*. 2015;15:10. doi:10.1186/s12906-015-0527-5

18. Li X, Jin Q, Wu Y, et al. Tetrandrine regulates hepatic stellate cell activation via TAK1 and NF-κB signaling. *Int Immunopharmacol*. 2016;36:263–270. doi:10.1016/j.intimp.2016.04.039
19. Gao S, Cui Y, Yu C, et al. Tetrandrine exerts antidepressant-like effects in animal models: role of brain-derived neurotrophic factor. *Behav. Brain Res*. 2013;238:79–85. doi:10.1016/j.bbr.2012.10.015
20. Yuan X, Tong B, Dou Y, et al. Tetrandrine ameliorates collagen-induced arthritis in mice by restoring the balance between Th17 and Treg cells via the aryl hydrocarbon. *Biochem Pharmacol*. 2016;101:87–99. doi:10.1016/j.bcp.2015.11.025
21. Li X, Wu Z, He B, et al. Tetrandrine alleviates symptoms of rheumatoid arthritis in rats by regulating the expression of cyclooxygenase-2 and inflammatory factors. *Exp Ther Med*. 2018;16:2670–2676. doi:10.3892/etm.2018.6498
22. Jang BC. Tetrandrine has anti-adipogenic effect on 3T3-L1 preadipocytes through the reduced expression and/or phosphorylation levels of C/EBP-a, PPAR-c, FAS, perilipin A, and STAT-3. *Biochem Biophys Res Commun*. 2017;494:422–423. doi:10.1016/j.bbrc.2016.05.150
23. Sakurai Y, Kolokoltsov A, Chen C, et al. Ebola virus. Two-pore channels control Ebola virus host cell entry and are drug targets for disease treatment. *Science*. 2015;347:995–998. doi:10.1126/science.1258758
24. Capuzzi S, Sun W, Muratov E, et al. Computer-aided discovery and characterization of novel Ebola virus inhibitors. *J Med Chem*. 2018;61:3582–3594. doi:10.1021/acs.jmedchem.8b00035
25. Lv Y, Wu Z, Chen L, et al. Neuroprotective effects of tetrandrine against vascular dementia. *Neural Regen Res*. 2016;11:454–459. doi:10.4103/1673-5374.179058
26. Corson T, Crews C. Molecular understanding and modern application of traditional medicines: triumphs and trials. *Cell*. 2007;130(5):769–774. doi:10.1016/j.cell.2007.08.021
27. Guo L, Luo S, Du Z, et al. Targeted delivery of celastrol to mesangial cells is effective against mesangioproliferative glomerulonephritis. *Nat Commun*. 2017;8(1):878. doi:10.1038/s41467-017-00834-8
28. Kang S, Park T, Chen X, et al. Tunable physiologic interactions of adhesion molecules for inflamed cell-selective drug delivery. *Biomaterials*. 2011;32(13):3487–3498. doi:10.1016/j.biomaterials.2011.01.046
29. Li X, Xie S, Pan Y, et al. Preparation, characterization and pharmacokinetics of doxycycline hydrochloride and florfenicol polyvinylpyrroliddone microparticle entrapped with hydroxypropyl-β-cyclodextrin inclusion complexes suspension. *Colloids Surf B*. 2016:634–642. doi:10.1016/j.colsurfb.2016.02.027
30. Gao L, Chen Y, Zhang N, et al. Intracoronary infusion of Wharton's jelly-derived mesenchymal stem cells in acute myocardial infarction: double-blind, randomized controlled trial. *BMC Med*. 2015. doi:10.1186/s12916-015-0399-z
31. Chen J, Gong Y, Liu J, et al. Synthesis and biological evaluation of substituted phenylpyrazole oleanane derivatives as inhibitors of glycogen phosphorylase. *Drug Discoveries Ther*. 2008;2(2):115–121. doi:10.1002/cbdv.200890117
32. Qu D, He J, Liu C, et al. Triterpene-loaded microemulsion using Coix lacryma-jobi seed extract as oil phase for enhanced antitumor efficacy: preparation and in vivo evaluation. *Int j Nanomed*. 2014;9(1):109–119. doi:10.2147/IJN.S54796
33. Chen Y, Qu D, Fu R, et al. A Tf-modified tripterine-loaded coix seed oil microemulsion enhances anti-cervical cancer treatment. *Int j Nanomed*. 2018;13:7275–7287. doi:10.2147/IJN.S182475
34. Chen Y, Guo M, Qu D, et al. Furin-responsive triterpenine-based liposomal complex enhances anticervical cancer therapy through size modulation. *Drug Delivery*. 2020;27(1):1608–1624. doi:10.1080/10717544.2020.1827086
35. Chen Y, Yuan L, Congyan L, et al. Antitumor activity of tripterine via cell-penetrating peptide-coated nanostructured lipid carriers in a prostate cancer model. *Int j Nanomed*. 2013;8. doi:10.2147/IJN.S51621
36. Qu D, Wang L, Liu M, et al. Oral nanomedicine based on multicomponent microemulsions for drug-resistant breast cancer treatment. *Biomacromolecules*. 2017;18(4):1268–1280. doi:10.1021/acs.biomac.7b00011
37. Ding Q, Mingjian L, Mengmeng H, et al. Octanoyl galactose ester-modified microemulsion system self-assembled by coix seed components to enhance tumor targeting and hepatoma therapy. *Int j Nanomed*. 2017;12:2045–2059. doi:10.2147/IJN.S125293
38. Qu D, Wang L, Qin Y, et al. Non-triggered sequential-release liposomes enhance anti-breast cancer efficacy of STS and celastrol-based microemulsion. *Biomater. Sci*. 2018;6(12):3284–3299. doi:10.1039/c8bm00796a
39. Li P, Zhou X, Qu D, et al. Preliminary study on fabrication, characterization and synergistic anti-lung cancer effects of self-assembled micelles of covalently conjugated celastrol-polyethylene glycol-ginsenoside Rh2. *Drug Deliv*. 2017;24(1):834–845. doi:10.1080/10717544.2017.1326540
40. Wong S, Kellaway I, Murdan S. Enhancement of the dissolution rate and oral absorption of a poorly water soluble drug by formation of surfactant-containing microparticles. *Int J Pharm*. 2006;317(1):61–68. doi:10.1016/j.ijpharm.2006.03.001
41. Guang H, Zhao Q, Du B, et al. Platelet-rich plasma protects human keratinocytes from UVB-induced apoptosis by attenuating inflammatory responses and endoplasmic reticulum stress. *J Cosmet Dermatol*. 2023;22(4):1327–1333. doi:10.1111/jocd.15559
42. Ceylan S. An in vitro evaluation of Genipin-crosslinked and Hypericum perforatum incorporated novel membranes for skin tissue engineering applications. *J Appl Polym Sci*. 2021;138. doi:10.1002/app.51385
43. Poley M, Chen G, Sharf-Pauker N, et al. Sex-based differences in the biodistribution of nanoparticles and their effect on hormonal, immune, and metabolic function. *Adv Nano Biomed Res*. 2022;2(12). doi:10.1002/anbr.202200089
44. Haney M, Yuan H, Shipley S, et al. Biodistribution of biomimetic drug carriers, mononuclear cells, and extracellular vesicles, in nonhuman primates. *Adv Biol*. 2021;6(2):e2101293. doi:10.1002/adbi.202101293
45. Song G, Tarrant T, White T, et al. Roles of chemokines CCL_2 and CCL_5 in the pharmacokinetics of PEGylated liposomal doxorubicin in vivo and in patients with recurrent epithelial ovarian cancer. *Nanomed Nanotechnol Biol Med*. 2015;11(7):1797–1807. doi:10.1016/j.nano.2015.05.007
46. Gonzalezvillasana V, Rodriguezaguayo C, Arumugam T, et al. Bisphosphonates inhibit stellate cell activity and enhance antitumor effects of nanoparticle albumin-bound paclitaxel in pancreatic ductal adenocarcinoma. *Mol Cancer Ther*. 2014;13(11):2583. doi:10.1158/1535-7163.MCT-14-0028
47. Kim S, Noh Y, Kang T, et al. Synthetic vaccine nanoparticles target to lymph node triggering enhanced innate and adaptive antitumor immunity. *Biomaterials*. 2017;130:56–66. doi:10.1016/j.biomaterials.2017.03.034
48. Lau U, Saxer S, Lee J, et al. Direct write protein patterns for multiplexed cytokine detection from live cells using electron beam lithography. *Acs Nano*. 2016;10(1):723–729. doi:10.1021/acsnano.5b05781
49. Koonce N, Quick C, Hardee M, et al. Combination of gold nanoparticle-conjugated tumor necrosis factor-α and radiation therapy results in a synergistic antitumor response in murine carcinoma models. *Int J Radiat Oncol Biol Phys*. 2015;93(3):588–596. doi:10.1016/j.ijrobp.2015.07.2275
50. Wajant H, Pfizenmaier K, Scheurich P. Tumor necrosis factor signaling. *Cell Death Differ*. 2003;10(1):45–65. doi:10.1038/sj.cdd.4401189

51. Wang X, Lin Y. Tumor necrosis factor and cancer, buddies or foes? *Acta Pharmacol Sin*. 2010;29(11):1275–1288. doi:10.1111/j.1745-7254.2008.00889.x
52. Balkwill F. Tumor necrosis factor or tumor promoting factor? *Cytokine Growth Factor Rev*. 2002;13(2):135–141. doi:10.1016/s1359-6101(01)00020-x
53. Esther S, Tsipi M, Polina W, et al. Inflammatory mediators in breast cancer: coordinated expression of TNFα & IL-1β with CCL_2 & CCL_5 and effects on epithelial-to-mesenchymal transition. *BMC Cancer*. 2011;11(1):130. doi:10.1186/1471-2407-11-130
54. Komohara Y, Fujiwara Y, Ohnishi K, et al. Tumor-associated macrophages: potential therapeutic targets for anti-cancer therapy. *Adv. Drug Delivery Rev*. 2016;99(Pt B):180–185. doi:10.1016/j.addr.2015.11.009
55. Bunimovich-Mendrazitsky S, Halachmi S, Kronik N. ImprovingBacillus Calmette-Guérin (BCG) immunotherapy for bladder cancer by adding interleukin 2 (IL-2): a mathematical model. *Math Med Biol*. 2016;33(2):159–188. doi:10.1093/imammb/dqv007
56. Wu J, Cui T, Yin C. Co-delivery of doxorubicin and interleukin-2 via chitosan-based nanoparticles for enhanced antitumor efficacy. *Acta Biomater*. 2017;47:81–90. doi:10.1016/j.actbio.2016.10.012
57. Kong H, Zhuo C, Yi K, et al. Hepatocyte-confined CRISPR/Cas9-based nanocleaver precisely eliminates viral DNA for efficient and safe treatment of hepatitis B virus infection. *Nano Today*. 2023:53. doi:10.1016/j.nantod.2023.102040
58. Kong H, Ju E, Yi K, et al. Advanced nanotheranostics of CRISPR/Cas for viral hepatitis and hepatocellular carcinoma. *Adv Sci*. 2021;8. doi:10.1002/advs.202170163